2024 IEEE Ultrasonics, Ferroelectrics, and Frequency Control Joint Symposium (UFFC-JS) | 979-8-3503-7190-1/24/$31.00 ©2024 IEEE | DOI: 10.1109/UFFC-JS60046.2024.10793609

Regularized Phase Gradient Analysis for Reverberant Shear Wave Elastography

Edmundo A. Miranda[†], Sebastian Merino[†], Juvenal Ormachea[⋆], Kevin J. Parker[§] and Roberto Lavarello[†]
[†]Laboratorio de Imágenes Médicas, Pontificia Universidad Católica del Perú, Lima, Peru
[⋆]Verasonics. Inc., Seattle, WA, USA
[§]Department of Electrical and Computer Engineering, University of Rochester, Rochester, NY, USA

***Abstract*—Reverberant shear wave elastography (R-SWE) evaluates tissue stiffness by creating a reverberant shear wave field in all directions and estimating the shear wave speed (SWS). A previous study established a linear relationship between the field's phase and the local wave number through the phase gradient (PG) method. This study introduces regularization into R-SWE to enhance the quality of the SWS maps across frequencies. Two regularization methods were analyzed: the single-channel Total Variation (TV) and the multi-frequency channel-based Total Nuclear Variation (TNV). The regularization framework involves unwrapping the phase in axial and lateral directions, calculating the ℓ_2-norm of the phase gradient, and proposing a minimizing cost function to address the denoising problem. Metrics were compared to PG with data from simulated and breast phantoms. Results show that regularized methods visually improved the quality of the SWS images while reducing the variability of the estimations. The contrast-to-noise ratio (CNR) was used as an overall metric. For the simulations, the average CNR values were 7.58 (PG-TNV), 2.38 (PG-TV) and 0.88 (PG). For the breast phantom, the CNR values were 4.36 (PG-TNV), 3.01 (PG-TV) and 2.39 (PG). These results suggest that regularization in R-SWE improves SWS imaging, with PG-TNV producing the best SWS maps across all frequency channels, enhancing the trade-off between variability and spatial resolution by incorporating information from multiple frequencies.**

***Index Terms*—Reverberant shear wave elastography, shear wave speed, regularization, total variation, total nuclear variation, multi-frequency elastography.**

I. Introduction

Elastography is a medical imaging approach to assess the biomechanical properties of tissues. One of the largest group of elastography techniques are based on shear wave propagation, estimating the shear wave speed (SWS), thus the stiffness of the medium [1]. Nevertheless, these techniques are affected by wave reflections due to organ boundaries and inhomogeneities [2]. The reverberant shear wave elastography (R-SWE) was proposed as an alternative since it leverages the reflected waves using external vibration sources to generate a reverberant shear wave field within the tissue [3].

Moreover, R-SWE yields the SWS by applying a relatively simple 2D autocorrelation estimator [4]. Nevertheless, it is limited by the window size, thus affecting its resolution. To overcome this, a new estimator labeled Phase Gradient (PG) was proposed which exploits the linear relationship between the field's phase and the local wave number, demonstrating lower sensitivity to imperfections in the reverberant field and requiring smaller window sizes [5].

Leveraging this relation, this study aims to introduce regularization into R-SWE to enhance the quality of the SWS maps across frequencies. Two regularization methods based on the Total Variation (TV) and the Total Nuclear Variation (TNV) were explored considering noise removal and edge preservation.

II. Methods

A. Reverberant Shear Wave Elastography (R-SWE)

A reverberant shear wave field can be described as the superposition of plane shear waves propagating in random directions, thus the particle velocity is defined as follows [4]

$$V(\bar{\epsilon},t)=\sum_{q,l}\hat{n}_{ql}v_{ql}e^{i(k\hat{n}_q\cdot\bar{\epsilon}-\omega_o t)}, \tag{1}$$

where $\hat{n}_{ql}$ is the random unit vector of the particle velocity v_{ql}, with $\hat{n}_q$ describing the direction of the wave propagation with a wave number k and a radial frequency ω_o.

Typically, the local wave number k is estimated by fitting a windowed 2D autocorrelation to spherical Bessel functions of the first kind of zero and first order [6]. Finally, given the excitation frequency f, the shear wave speed (SWS) is obtained by

$$c_s=2\pi\cdot f/k. \tag{2}$$

B. Phase Gradient Method (PG)

The phase gradient (PG) estimator was introduced to enhance spatial resolution, requiring smaller window sizes [5]. The phase can be shown to be proportional to the wave number, defined as follows

$$\hat{\phi}(x,z)\cong k_x x+k_z z+\phi_0, \tag{3}$$

where $\hat{\phi}$ is the unwrap phase within a small window. Thus, by taking the gradient of the phase in the axial and lateral directions we can obtain

$$\nabla_z\hat{\phi}_z=k_z,\nabla_x\hat{\phi}_x=k_x \tag{4}$$

where k_z and k_x correspond to the wavenumber in the axial and lateral directions, respectively. Then

$$(\nabla_z\hat{\phi}_z)^2+(\nabla_x\hat{\phi}_x)^2=k_x^2+k_z^2=k^2 \tag{5}$$

Lastly, the SWS is calculated using Eq. (2).

C. Regularized Phase Gradient

We present a regularized framework of the PG estimator, by leveraging the ℓ_2 norm of the phase gradient and considering the unwrap versions of the phase in the axial and lateral directions

$$\|\nabla\hat{\phi}\|_2 = \sqrt{(\nabla_z\hat{\phi}_z)^2 + (\nabla_x\hat{\phi}_x)^2}. \tag{6}$$

Thus, an average of the phase gradients $\|\nabla\hat{\phi}\|_2$ can be ensembled in Φ. Then, considering $\boldsymbol{K}$ as the wave number at each spatial location, it can be reformulated as an inverse problem where regularization is introduced

$$\min_{\boldsymbol{K}} \ \frac{1}{2}\|\boldsymbol{K} - \Phi\|_2^2 + \mu\mathcal{R}(\boldsymbol{K}). \tag{7}$$

1) Total Variation Method (PG-TV): The first approach is based on spatial regularization of the Φ_r term at each vibration frequency f_r by using the single-channel total variation, minimizing

$$\min_{\boldsymbol{K}_r} \ \frac{1}{2}\|\Phi_r - \boldsymbol{K}_r\|_2^2 + \mu\text{TV}(\boldsymbol{K}_r), \tag{8}$$

with $\boldsymbol{K}_r \in \mathbb{R}^{m\times n}$ as the denoised wave number map. μ is the regularization parameter. The TV is defined as follows

$$\text{TV}(u) = \sum_{i,j}\sqrt{(D_x u)^2 + (D_z u)^2}, \tag{9}$$

where D_x and D_z are the discrete derivatives operators. The objective function defined in Eq. (8) is minimized using the Iterative Re-weighted Least Squares method [7].

2) Total Nuclear Variation Method (PG-TNV): The second approach is a multi-frequency approach based on joint denoising at all frequency channels, using the total nuclear variation and minimizing

$$\min_{\boldsymbol{K}} \ \frac{1}{2}\|\Phi - \boldsymbol{K}\|_2^2 + \mu\text{TNV}(\boldsymbol{K}), \tag{10}$$

where $\boldsymbol{K} \in \mathbb{R}^{m\times n\times p}$ and $\Phi \in \mathbb{R}^{m\times n\times p}$ are the tensors of local shear numbers $\boldsymbol{K}_r$ and phase gradients Φ_r, respectively. The TNV prior is based on exploiting geometrical structures among all channels and is defined as

$$\text{TNV}(u) = \sum_{i,j}\|\mathcal{J}(u)\|_*, \tag{11}$$

where $\mathcal{J}$ stands for the Jacobian array of D_x and D_z for all channels and $\|\ \|_*$ denotes the nuclear norm, defined as the sum of the singular values of the array. The TNV promotes parallelism among frequency channels by edge coupling and gradient alignment of all the Φ_r maps, considering the reconstructed maps must exhibit the same geometry. The objective function in Eq. (10) can be solved by proximal operators and the primal-dual algorithm [8].

D. Experiments

Simulations were generated in MATLAB 2024a (MathWorks Inc., Natick, MA, USA) using a 3D space of $50 \times 50 \times 50$ mm^3 with a resolution of 0.2 mm. The simulations consisted of a fully elastic medium containing a spherical inclusion of 10 mm radius at 25 mm depth. The SWS ideal values were set to be 4.5 m/s and 2.5 m/s for the inclusion and background, respectively. The vibration frequencies ranged from 500 to 1000Hz in steps of 100Hz.

Additionally, data from a CIRS breast phantom used in [5], acquired with a Verasonics system (Vantage-128TM, Verasonics, Kirkland, WA, USA), an L7-4 linear transducer, and multiple embedded vibration sources with frequencies of 400, 600, and 900 Hz was used. The reported SWS by the manufacturer were 3.65 m/s and 2.58 m/s for the inclusion and background, respectively.

E. Evaluation of the SWS maps

The SWS maps were reconstructed by the PG, PG-TV and PG-TNV techniques with a fixed window of 15×15. An additional 7×7 average filter was applied for the PG method. Metrics of the inclusion and background such as mean and standard deviation and contrast-to-noise ratio (CNR) were calculated. The SWS maps presented were generated with the μ value that minimizes the estimation bias of the image.

III. Results

A. Simulated Phantom

Fig. 1 shows the SWS maps for the fully elastic medium and the metrics are detailed in Table II. Moreover, Fig. 2 shows the dispersion graph of the SWS at all frequencies. Overall, the regularization methods (PG-TV and PG-TNV) yield an enhanced reconstruction over PG. The CNR across frequencies was calculated (see Fig. 5a), showing an enhanced performance by PG-TV and PG-TNV.

B. Breast Phantom

The SWS maps are shown in Fig. 3 for each frequency. Furthermore, the dispersion of the estimated SWS for the inclusion and background are displayed in Fig. 4. Similarly to the simulations, PG-TV and PG-TNV achieved a superior CNR compared to PG (see Fig. 5b). All the metrics are summarized in Table I.

TABLE I
MEAN, STD AND CNR OF THE BREAST PHANTOM USING THE PG, PG-TV AND PG-TNV METHODS. GROUND-TRUTH VALUES: 3.65 M/S (INCLUSION) AND 2.58 M/S (BACKGROUND).

Method	Metric	**400 Hz**	**600 Hz**	**900 Hz**
3***PG**	SWS in. [m/s]	2.96±0.44	3.56±0.35	4.10±0.44
	SWS bg. [m/s]	2.24±0.23	2.21±0.24	2.56±0.42
	CNR	1.47	3.19	2.51
3***PG-TV**	SWS in. [m/s]	2.86±0.18	3.27±0.21	3.75±0.23
	SWS bg. [m/s]	2.33±0.13	2.28±0.12	2.66±0.37
	CNR	2.44	4.09	2.51
3***PG-TNV**	SWS in. [m/s]	2.83±0.12	3.32±0.16	3.71±0.15
	SWS bg. [m/s]	2.26±0.07	2.26±0.08	2.62±0.31
	CNR	4.12	5.82	3.15

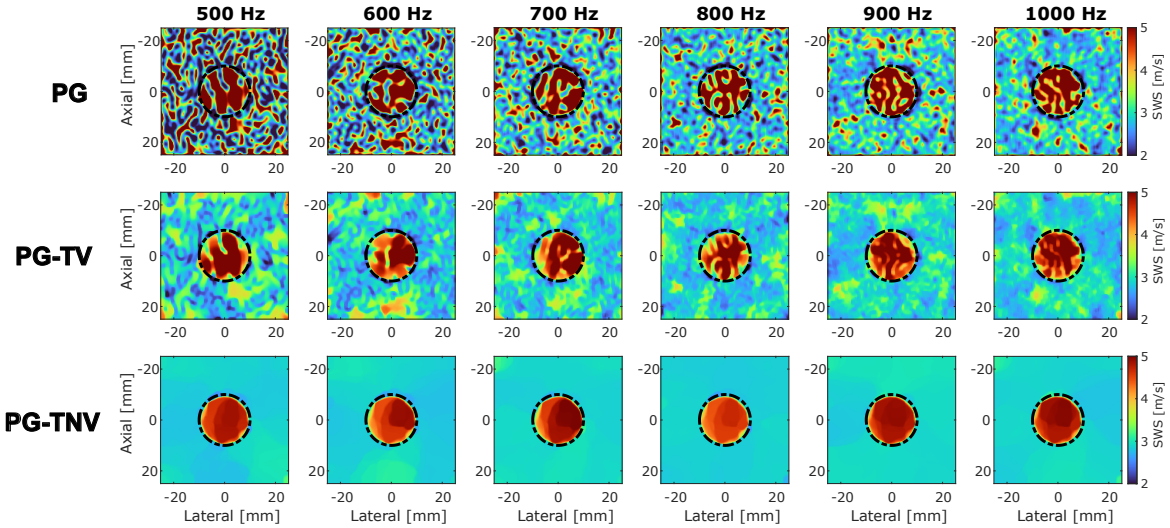

Fig. 1. Reconstructed SWS maps from the simulated elastic phantom with the PG, PG-TV and PG-TNV methods across different vibration frequencies.

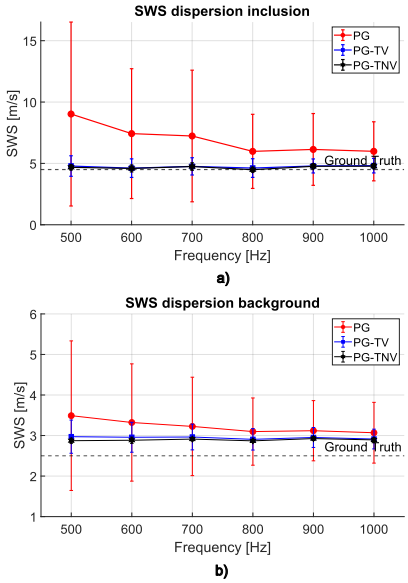

Fig. 2. SWS dispersion across frequencies by the PG, PG-TV and PG-TNV methods for the (a) inclusion and (b) background regions of the elastic simulated phantom.

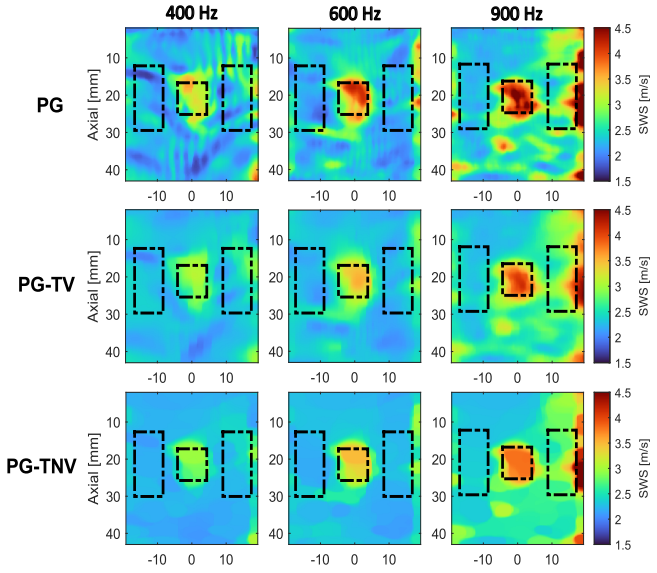

Fig. 3. Reconstructed SWS maps from the breast phantom with the PG, PG-TV and PG-TNV methods across different vibration frequencies.

IV. Discussion

In the simulation (see Fig. 1), the regularization techniques (PG-TV and PG-TNV) generated visual improvements in the SWS maps compared to the PG approach. In particular, the multi-frequency PG-TNV method yielded smoother images across all frequencies providing a stable SWS mean value close to the ground truth for the inclusion and background, while significantly reducing the variability of the estimations (see Fig. 2 and Table II). Consequently, PG-TNV achieved the best performance of all the methods as measured with the CNR (see Fig. 5a), reporting an average CNR value of 7.58, compared to 2.38 (PG-TV) and 0.88 (PG).

In the breast phantom, regardless of the scarcity of frequency channels when compared to the simulations, the multi-frequency approach (PG-TNV) achieved SWS maps with fewer artifacts and a smoother background (see Fig. 3). Moreover, the SWS estimations were in line with the phantom datasheet. In the inclusion, the average SWS values were 3.54 ± 0.41 m/s (PG), 3.29 ± 0.21 m/s (PG-TV) and 3.29 ± 0.14 m/s (PG-TNV). In the background, the average SWS values were 2.34 ± 0.31 m/s (PG), 2.42 ± 0.23 m/s (PG-TV) and 2.38 ± 0.18 m/s (PG-TNV). Lastly, the CNR was used as an overall metric for the quality of the SWS maps (see Fig. 5b), where PG-TNV achieved the highest average CNR, which was 4.36, compared to 3.01 and 2.39 by PG and PG-TV, respectively.

TABLE II

MEAN, STD AND CNR OF THE SIMULATED PHANTOM USING THE PG, PG-TV AND PG-TNV METHODS. GROUND-TRUTH VALUES: 4.5 M/S (INCLUSION) AND 2.5 M/S (BACKGROUND).

Method	Metric	**500 Hz**	**600 Hz**	**700 Hz**	**800 Hz**	**900 Hz**	**1000 Hz**
3***PG**	SWS in. [m/s]	9.02 ± 7.49	7.43 ± 5.29	7.23 ± 5.36	5.98 ± 3.02	6.14 ± 2.93	5.99 ± 2.41
	SWS bg. [m/s]	3.49 ± 1.84	3.32 ± 1.45	3.22 ± 1.21	3.1 ± 0.83	3.12 ± 0.74	3.07 ± 0.75
	CNR	0.72	0.75	0.73	0.92	1.0	1.16
3***PG-TV**	SWS in. [m/s]	4.79 ± 0.84	4.61 ± 0.76	4.76 ± 0.7	4.62 ± 0.76	4.79 ± 0.57	4.82 ± 0.59
	SWS bg. [m/s]	2.97 ± 0.41	2.96 ± 0.37	2.96 ± 0.32	2.91 ± 0.26	2.95 ± 0.25	2.91 ± 0.24
	CNR	1.95	1.97	2.33	2.13	2.96	2.96
3***PG-TNV**	SWS in. [m/s]	4.68 ± 0.21	4.59 ± 0.28	4.75 ± 0.3	4.49 ± 0.2	4.76 ± 0.2	4.77 ± 0.21
	SWS bg. [m/s]	2.87 ± 0.06	2.88 ± 0.08	2.91 ± 0.04	2.87 ± 0.02	2.92 ± 0.05	2.89 ± 0.05
	CNR	8.16	5.83	5.99	7.93	8.97	8.64

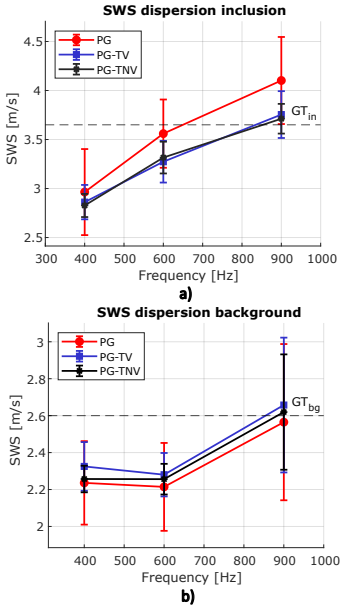

Fig. 4. SWS dispersion across frequencies by the PG, PG-TV and PG-TNV methods for the (a) inclusion and (b) background regions of the breast phantom.

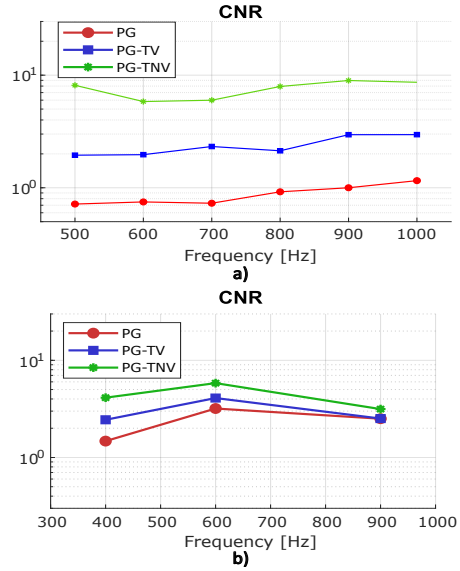

Fig. 5. CNR of the SWS maps with the PG, PG-TV and PG-TNV methods for (a) the simulated phantom and (b) the breast phantom.

V. CONCLUSIONS

A regularization framework for R-SWE was introduced and solved using the single-channel total variation (PG-TV) and the total nuclear variation (PG-TNV), the latter for a multi-frequency approach. Initial results from simulated and breast phantoms suggest the regularization approaches outperformed the previous estimator (PG), yielding enhanced SWS maps with better delineation of the inclusions and less variability in the estimations. In particular, incorporating spatial information by the multi-frequency PG-TNV allows the reconstruction of visually superior SWS maps with a greater CNR across all frequencies.

ACKNOWLEDGMENT

This work was supported by Pontificia Universidad Católica del Peru under the research grant PUCP CAP 2023-F-0020.

REFERENCES

[1] J. Ormachea and K. J. Parker, "Elastography imaging: the 30 year perspective," *Physics in Medicine & Biology*, vol. 65, no. 24, p. 24TR06, 2020.

[2] M. Bruce, O. Kolokythas, G. Ferraioli, C. Filice, and M. O'Donnell, "Limitations and artifacts in shear-wave elastography of the liver," *Biomedical engineering letters*, vol. 7, pp. 81–89, 2017.

[3] K. J. Parker, J. Ormachea, F. Zvietcovich, and B. Castaneda, "Reverberant shear wave fields and estimation of tissue properties," *Physics in Medicine & Biology*, vol. 62, no. 3, p. 1046, 2017.

[4] J. Ormachea, B. Castaneda, and K. J. Parker, "Shear wave speed estimation using reverberant shear wave fields: implementation and feasibility studies," *Ultrasound in Medicine & Biology*, vol. 44, no. 5, pp. 963–977, 2018.

[5] J. Ormachea and K. Parker, "Reverberant shear wave phase gradients for elastography," *Physics in Medicine & Biology*, vol. 66, no. 17, p. 175001, 2021.

[6] J. Ormachea and F. Zvietcovich, "Reverberant shear wave elastography: a multi-modal and multi-scale approach to measure the viscoelasticity properties of soft tissues," *Frontiers in Physics*, vol. 8, p. 606793, 2021.

[7] P. Rodríguez, "Total variation regularization algorithms for images corrupted with different noise models: a review," *Journal of Electrical and Computer Engineering*, vol. 2013, no. 1, p. 217021, 2013.

[8] E. A. Miranda, A. Basarab, and R. Lavarello, "Multifrequency joint reconstruction of ultrasonic attenuation images," in *2023 IEEE International Ultrasonics Symposium (IUS)*. IEEE, 2023, pp. 1–4.